JOURNAL OF PROPULSION AND POWER
Vol. 10, No. 3, May–June 1994

Experimental Investigation of Counter-Rotating Propfan Flutter at Cruise Conditions

Oral Mehmed* and Anatole P. Kurkov†
NASA Lewis Research Center, Cleveland, Ohio 44135

This article presents wind-tunnel experimental flutter results, at transonic relative flows, for a 0.62-m-diam composite propfan model. A blade row that fluttered was tested alone, and with a stable aft counter-rotating blade row. The major objectives of the experiment were to study the effect of the second blade row on the row in flutter, and to investigate the flutter. Results show that the second row had a small stabilizing effect. Two distinct flutter modes were found within the operating regime of the rotor; both apparently single-degree-of-freedom instabilities, associated respectively with the first and second natural blade modes. For both flutter modes, flutter boundary, frequency, nodal diameter, and blade displacement data are given. The blade displacement data, obtained with an optical method, gives an indication of the flutter mode shape at a span near the blade tip.

Introduction

PROPFANS were under development because they have significantly higher propulsion efficiency than turbofans at the same cruise speeds. Interest started with single row (SR) propfans and changed to counter-rotating (CR) propfans because they have even greater efficiency.[1] The unducted fan was a two-row CR propfan concept being developed. During aero/acoustic wind-tunnel testing of unducted fan research models at cruise speeds, several blade designs fluttered.[2] Some trends and characteristics of the flutter were different than those previously found for SR propfans.

SR propfan unstalled flutter has been investigated experimentally.[3–5] From these experiments the type of flutter (classical) and the sensitivity of the flutter to stage parameters were identified. Also, flutter analyses have been developed for SR propfans.[6,7] The flutter analyses developed for SR propfans have been used for the design of CR propfans.[8] The accuracy of such flutter predictions would change if the stability characteristics of one blade row are significantly changed by the second row. The predictions would be less safe if the second row caused a decrease in stability.

The present experiment was planned to help guide the development of flutter analyses for CR propfans and further investigate propfan flutter. The main object of the experiment was to study the effect of a stable CR propfan blade row on the stability of a row that fluttered. The unstable row used for the experiment was known to flutter from earlier aero/acoustic wind-tunnel tests.

This article presents new flutter boundary data for a fluttering propfan blade row (called F21) tested alone, and with a stable aft CR blade row (called A21). The terms blade row and rotor will be used interchangeably, and the F21 and A21 rows will be referred to as the forward and aft rows, respectively. The blades were research models for an Unducted Fan engine.[9] Two distinct flutter modes were found. For both flutter modes, flutter boundary, frequency, nodal diameter, and blade displacement data are given. We use the change in the F21 flutter boundaries for the single and dual rows to determine how the aft row changed the stability of the forward row.

A nonintrusive optical system was used to measure the blade vibrations at flutter. This system provided complete blade-to-blade phase information. It also provided an indication of the flutter mode shape at a blade span near the tip. Conventional blade mounted strain gauges were used to measure flutter frequency. The optical system description and detailed spectral results have previously been reported.[10] For completeness, a brief description of the optical system, frequency, blade displacement, and nodal diameter data for the front row alone are repeated herein.

Apparatus and Procedures

The experiment was done in the NASA Lewis 8- by 6-ft Supersonic Wind Tunnel.[11] The tunnel has porous walls and a rectangular test section that is 2.44 m high and 1.83 m wide. The freestream Mach numbers ranged from 0.50 to 0.84 during the experiment. The Lewis Counter-Rotating Pusher Propeller Test Rig[12] was floor strut mounted in the tunnel, as shown in Fig. 1. Two rotors are driven by independently controlled air turbines, allowing different and independent rotational speeds. The forward and aft blades were designed for the same speed, but were operated at different speeds to obtain the flutter data. There are 13 F21 blades in the forward row and 10 A21 blades in the aft. The propeller diameters are nominally 0.62 m (2 ft). Table 1 gives some of the design and model characteristics.

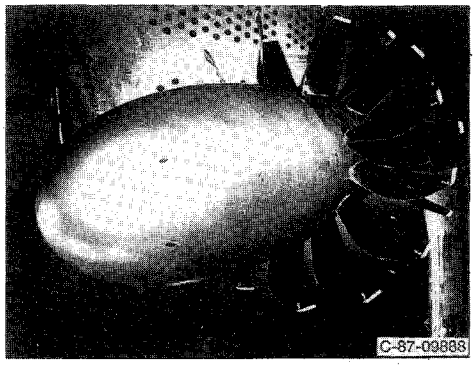

Fig. 1 F21/A21 model installed in the NASA Lewis 8- by 6-ft Supersonic Wind Tunnel.

Received Feb. 28, 1993; presented as Paper 93-1634 at the AIAA/ASME/ASCE/AHS/ASC 34th Structures, Structural Dynamics, and Materials Conference, San Diego, CA, April 19–21, 1993; revision received Dec. 8, 1993; accepted for publication Dec. 9, 1993.

*Senior Research Engineer. Member AIAA.
†Senior Research Engineer.

Table 1 F21/A21 design and model characteristics

	F21	A21
Number of blades	13[a]	10
Tip diameter, cm (in.)	61.80 (24.33)	59.66 (23.49)
Hub-to-tip ratio	0.429	0.423
Spacing between rows, cm (in.)	14.99 (5.90)	14.99 (5.90)
Design cruise Mach number	0.80	0.80
Design advance ratio	3.124	3.214
Design power coefficient[b]	2.79	2.79
Tip speed,[c] m/s (ft/s)	243.8 (800)	243.8 (800)
Aerodynamic tip sweep, deg	45	25

[a]Designed for 11 forward blades.
[b]Based on the forward row and using the annulus area.
[c]At nominal design cruise condition.

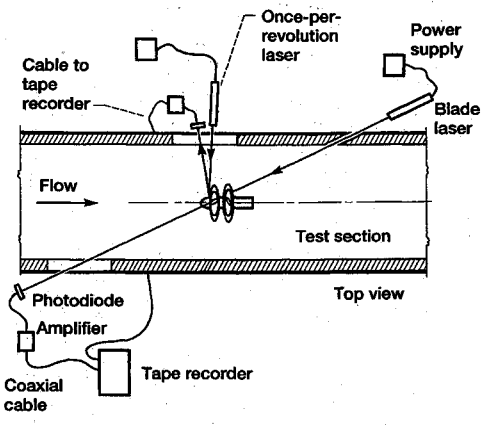

Fig. 2 Optical blade deflection measurement system diagram.

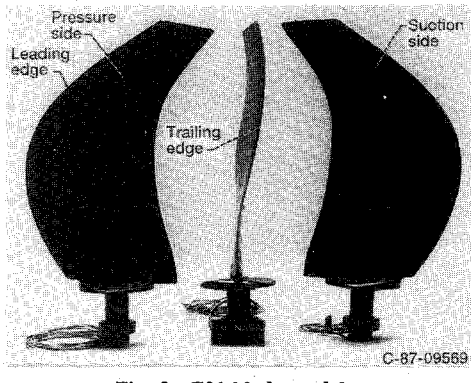

Fig. 3 F21 blade model.

An optical system, developed to measure deflections of unducted blades, was used to measure blade vibrations at flutter.[13] This system uses two laser beams as illustrated in Fig. 2. One beam is aimed across the blade path to a photodiode. Each time a blade interrupts the beam from reaching the diode a negative voltage pulse is created. The second beam is reflected to another photodiode when a small mirror on the blade hub rotates past it. This creates positive voltage pulses with spacing equal to the once-per-revolution time. The steady-state displacements are found by averaging, typically over 100 revolutions, the instantaneous blade positions relative to the once-per-revolution pulse. The dynamic displacements are found by subtracting the averaged steady-state displacements from the original blade positions. The optical displacement data were recorded on magnetic tape and processed after the experiment.

Figure 3 is a planform and edge-view photograph of an F21 model blade. The blade is constructed of a graphite/glass shell and a spar and shank of titanium. The wires at the blade base are from foil resistance strain gauges on the blade pressure surface. At the start there were a total of 12 blade gauges on the F21 rotor. However, nine gauge signals were lost early in the experiment.

Figure 4 shows the first three calculated in-vacuum nonrotating frequencies, and mode shapes for an F21 blade. The modes all have coupled motions, but the primary motions are used to describe them. The modes are first bending, second bending, and first torsion, respectively. The measured flutter frequencies and mode shapes, discussed later, fall close to those of the first and second calculated modes.

Except for the windmilling (unpowered rotor) flutter points, flutter was reached by manually powering the rotor to increase the forward rotor speed, at a fixed wind-tunnel Mach number and aft rotor power. The forward rotor speed was incremented in 20-rpm steps as flutter was approached. The windmilling points were reached by slowly increasing the tunnel Mach number. These procedures were reversed, but with haste, to get out of flutter. At powered points the rotor was automatically unpowered when a preselected strain limit was reached.

Results and Discussion

Experimental results are given at flutter for the F21 propfan model tested alone, and with the stable A21 CR blades in the aft row. Two distinct flutter modes were found. For both modes, flutter boundary, frequency, nodal diameter, and displacement data are discussed, in the order listed.

The measured stability boundaries for the F21 propfan in terms of the basic operating parameters (rotor speed vs freestream Mach number) are given in Fig. 5. Flutter conditions are given for three different blade setting angles and the single and dual rotors. The stable region is the area below the flutter boundary. The data shows that the stable region of operation decreases as the blade angle increases. Comparing the solid and dashed flutter boundaries, we see that at most conditions the unpowered aft rotor caused a small increase in the stability of the F21 rotor. The solid symbols above the dashed boundary are conditions where the aft rotor is powered, with increasing power moving toward the top of the figure. The F21 stability was increased further at these conditions. The effect of the aft row can be explained if we consider that the presence and powering of the aft row causes the magnitude of the local axial flow velocities into the front row to change. This in turn,

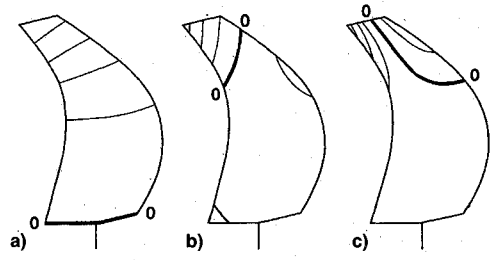

Fig. 4 F21 blade calculated nonrotating natural frequencies and mode shapes: a) mode 1 (159 Hz), b) mode 2 (375 Hz), and c) mode 3 (659 Hz).

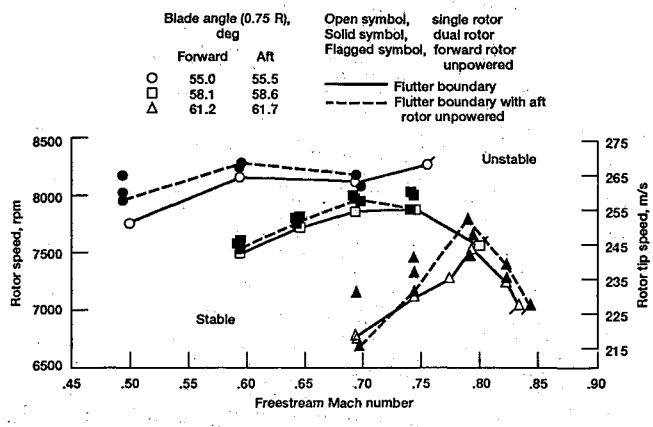

Fig. 5 F21 propfan flutter boundaries, rotor speed variation with freestream Mach number.

Table 2 Rotor power coefficient summary at flutter with the dual rotors

Blade angle (forward/aft), deg	Freestream Mach number	Power coefficient,[a] forward rotor, aft rotor unpowered[b]	Power coefficient,[a] (forward rotor/aft rotor), aft rotor at max power
55.0/55.5	0.50	2.40	2.37/1.97
	0.60	1.76	1.57/2.17
	0.70	0.60	0.34/1.02
58.1/58.6	0.60	2.35	2.23/2.50
	0.65	2.06	1.89/2.46
	0.70	1.63	1.41/2.07
	0.74	0.96	0.96/2.13
61.2/61.7	0.70	1.74	2.17/2.34
	0.74	1.72	1.88/2.26
	0.79	1.86	1.41/2.07
	0.82	1.04	0.54/1.33
	0.84	0	—

[a]Based on the forward row and using the annulus area.
[b]Power coefficient of aft rotor is zero.

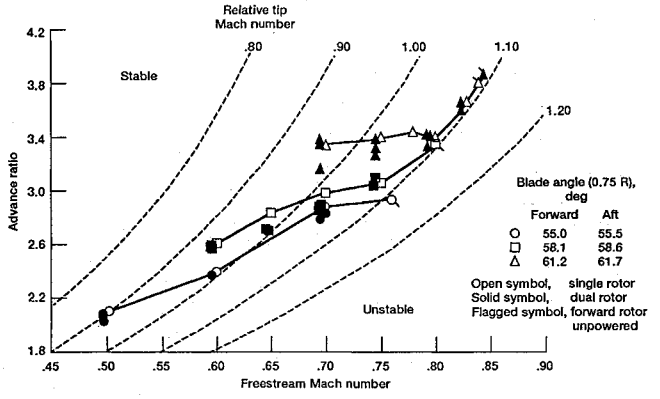

Fig. 6 F21 propfan flutter boundaries, advance ratio variation with freestream Mach number.

changes the angles of attack and relative velocities of the flow into the row because of induced flow. We suspect it is the change in one or both of these parameters that results in the increased stability of the front row.

Table 2 gives a summary of the power coefficients for both rotors, at the unpowered and the maximum powered aft rotor conditions. The power coefficient of each row is given by the equation

$$C_p = P/\rho n^3 d_{\text{tip}}^3 A$$

where C_p is the power coefficient, P is the power absorbed by the row, ρ is the freestream air density, n is the front row rotor speed, d_{tip} is the front row tip diameter, and A is the front row annular area. With this definition the ratio of power coefficients is equal to the ratio of row powers. Table 2 shows that the aft rotor was powered to significant levels relative to the forward rotor.

In Fig. 5, observe the slope differences between and the slope changes along the flutter boundaries. The boundary for the 55-deg blade angle has a small increase in flutter rpm with increasing freestream Mach number up to the unpowered flutter point at Mach 0.76. The same is true for the 58.1-deg blade angle boundary up to a Mach number of 0.75, but then a change occurs and the flutter rpm decreases with increasing freestream Mach number. The boundary for the 61.2-deg blade angle shows a greater rate of flutter rpm increase than the other boundaries up to a Mach of about 0.80. Then, a sudden change occurs and the flutter rpm decreases, similar to the boundary for the 58.1-deg blade angle. The cause for the slope changes, and differences along the boundaries are discussed later and are attributed to a change in the physics of the flutter and the modes along the boundaries, respectively.

To get a better physical understanding of what is happening, the flutter boundaries are redrawn in Fig. 6. Now the variation of advance ratio at flutter is shown with freestream Mach number. Advance ratio J is given by the expression

$$J = \pi V_{\text{axial}}/V_{\text{tip}}$$

where V_{axial} is the freestream velocity, and V_{tip} is the tip rotational velocity. Advance ratio is used because it is available data and is related to the angle of attack of the flow into the row at the blade tips. The expression relating the advance ratio and the angle of attack at any blade radius r is

$$\alpha = \beta - \arctan(J/\pi \times r_{\text{tip}}/r)$$

where α is the angle of attack at r, β is the blade angle of the deflected blade shape at r, and r_{tip} is the tip radius. Calculated contours of constant relative tip Mach number are also shown. Interestingly, all three boundaries appear to reach a limit at a relative tip Mach number of about 1.10. Once this Mach number is reached flutter occurs regardless of the value of angle of attack. It is inferred that this Mach number limit is the cause of the negative slopes in Fig. 5. Now consider the boundaries in Fig. 6 at relative tip Mach numbers less than 1.10. In this region a positive boundary slope indicates both a relative tip Mach number and an angle-of-attack change along the boundary. We see that the slope of the lower two boundaries is significantly greater than the slope of the upper boundary. This indicates that the change in angle of attack as relative tip Mach number varies is larger for the lower two boundaries compared to the upper boundary. As a matter of fact, the very small slope of the upper boundary means that the angle of attack is almost constant along the boundary. Thus, in this flow velocity region along the upper boundary, angle of attack appears to be a flutter limit regardless of the value of relative tip Mach number. A factor that may be causing the difference in sensitivity to angle of attack between the boundaries is a difference in flutter mode for the boundaries. It will be shown that the flutter mode associated with the lower two boundaries is second bending, and with the upper boundary it is first bending. From the slopes of the isodisplacement contours in Fig. 4, we see that the blade motion for the second bending mode (mode 2) has a large torsion component in the tip region compared to the first bending mode (mode 1). We conclude from Fig. 6 that the physics of the flutter is different at and below a relative tip Mach number of 1.10.

The flutter frequencies are shown on a Campbell diagram in Fig. 7. Also shown, for the first two modes, are the calculated in-vacuum single blade natural frequencies, and the nonrotating bench measured frequencies. The data shows that the flutter occurred in either of two distinct flutter modes. One flutter mode is near the first natural blade mode (the

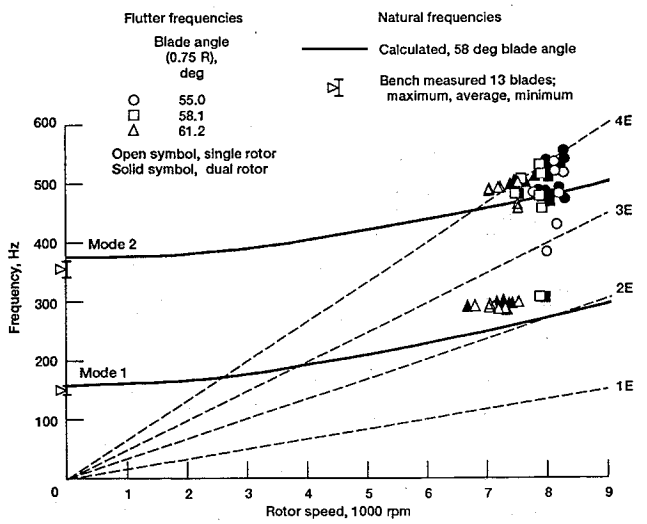

Fig. 7 F21 propfan measured flutter frequencies on a Campbell diagram.

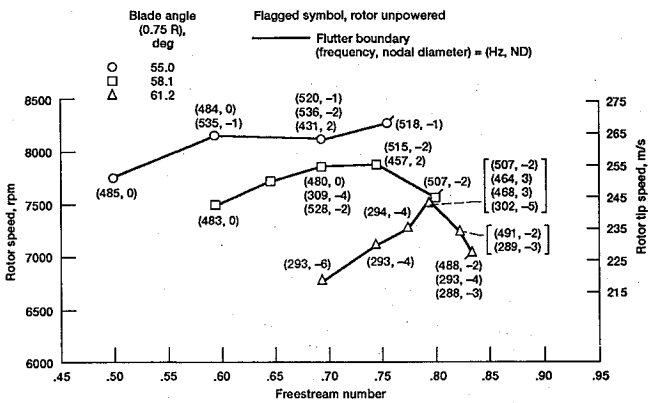

Fig. 8 F21 propfan flutter frequencies and nodal diameters on the single rotor flutter boundaries.

first bending mode) and the other is near the second (the second bending mode). In addition, some of the flutter points near the second natural mode fall close to the four-engine-order excitation line (for further details see Ref. 10). However, the displacement data obtained from the optical measurements show that none of these points have the phase relationship that is necessary for a four-engine-order forced response.

The flutter boundaries for the single rotor are revisited in Fig. 8 to show the variation of flutter frequency and nodal diameter along the boundaries. Nodal diameters are calculated from the average of the measured blade-to-blade phase angles around the rotor. The phase angles had large variation around the rotor, such that if measurements were taken from only a few blades (like is typically done when only strain gauges are used) an accurate value of nodal diameter would not have been obtained. The higher frequency flutter mode occurs along the entire two upper boundaries. In contrast, the frequency of the flutter mode changes along the lower boundary. The lower frequency flutter mode occurs along the positive slope portion, and the higher frequency flutter mode along the negative slope portion. The mode change is at about the 0.80 freestream Mach number, and this corresponds to the condition where the relative tip Mach number reaches the 1.10 limiting value in Fig. 6. There are also multiple nodal diameters and frequencies at some flutter conditions in Fig. 8. The spectral data[10] shows that all the modes listed at each condition went unstable at the same time. The mode of largest amplitude is shown at the top of each column. Readers interested in seeing details of the flutter response spectra are directed to Ref. 10.

An indication of the flutter mode shapes from the optical displacement measurements is shown in Fig. 9. The mode shapes, represented by the ratio of leading-edge to trailing-edge amplitudes, were measured at a blade span near the tip. Also shown, are in-vacuum calculated single blade results for the first two blade natural modes. These are at the two extremes of blade setting angle, 55 and 61.2 deg; and for the rotational speeds that span the experimental range associated with the blade angles. The variation in frequency for each calculated natural mode is caused by the change in rotational speed or blade angle, since these are in-vacuum calculations. Also, shown on the figure are the nodal diameters associated with each measured point. They were obtained from the optical displacement spectra.

The first group of measured points cluster near the calculated points for first natural mode and differ little in both frequency and mode shape from the calculated values. Hence, the measured points appear to be from a single-degree-of-freedom flutter mode associated with the first natural mode. The nodal diameters for this group of points range from -3 to -6. The variation of frequencies for the measured and calculated points is about the same.

The second group of measured points is clustered to the right and slightly below the points for the second calculated natural mode. Using the calculated points as a measure, the spread in frequency for this flutter mode is larger than can be attributed to the change in rotor speed or blade angle. However, the spread may be due to a variation of flutter frequency with nodal diameter. The measured and calculated mode shapes for this group are in closer agreement than those of the first group. These measured points also appear to be from a single-degree-of-freedom flutter mode, but are associated with the second natural mode. The nodal diameters for these points range from 0 to -2. There is only one point with a nodal diameter of 3.

The points not near the clusters associated with the two natural frequencies are, in general, secondary flutter responses of lower amplitude. These points have nodal diameters of 2 and 3, and would probably be associated with the second natural mode from their frequencies alone. However, their amplitude ratios show they are not associated with the second mode, and illustrate the wide range of amplitude ratios possible for nonintegral order, self-excited vibrations in transonic flow.

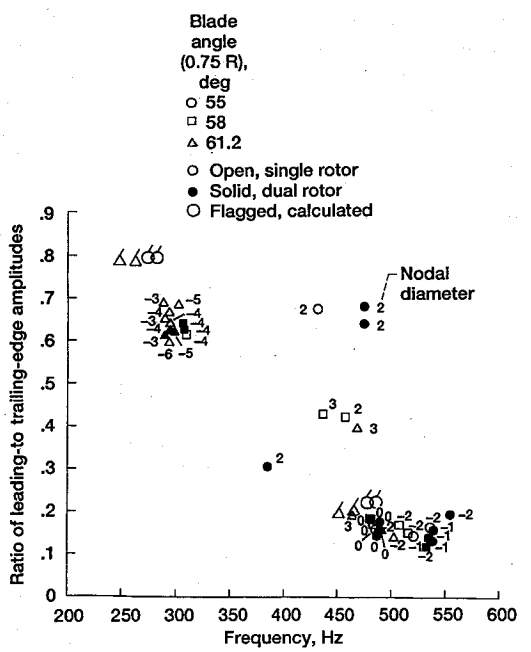

Fig. 9 Variation of average F21 blade leading-to-trailing-edge amplitude ratio and nodal diameter with flutter frequency.[11]

Concluding Remarks

A wind-tunnel experiment was done to determine the effect of a stable counter-rotating propfan blade row on the stability of a row that fluttered. The fluttering row was tested alone and with the stable blades in the aft row. A nonintrusive optical method, used to measure blade vibrations during flutter, provided complete blade-to-blade phase information and an indication of the flutter mode shapes. Conventional strain gauges were used to measure flutter frequency. Some major conclusions of the work are as follows:

1) The presence of a stable aft counter-rotating blade row had a small stabilizing effect on a fluttering blade row. The stability increased with increased power of the aft row.

2) Two distinct flutter modes occurred. One flutter mode was associated with the first, and the other with the second natural blade mode.

3) The dominant nodal diameters found were -3 to -6 for the lower frequency flutter mode, and 0 to -2 for the higher frequency mode.

4) At lower Mach numbers the flutter had a dependence on angle of attack and relative tip Mach number. But the angle-of-attack range was much smaller for the lower frequency flutter mode compared to the higher frequency flutter mode. However, when a relative tip Mach number of about 1.10 was reached it became the limiting parameter, and the flutter occurred independently of the value of the angle of attack.

5) Increasing the blade angle had a destabilizing effect.

It can be concluded from the experiment that flutter analyses developed for single rotor propfans should give conservative results when used for counter-rotating rows similar to the ones tested. More accurate analysis should include the effects of row interactions.

Acknowledgments

We are grateful to Robert J. Jeracki of the NASA Lewis Propulsion Systems Division, Propeller and Acoustics Technology Branch. He helped conduct the experiment, provided steady aerodynamic performance data from the experiment, and participated in useful discussions about the model and its performance. Also, thanks go to Durba V. Murthy of the University of Toledo, Toledo, Ohio. His suggestions and technical comments about the manuscript were very valuable.

References

[1]Mikkelson, D. C., Mitchell, G. A., and Bober, L. J., "Summary of Recent NASA Propeller Research," Aerodynamics and Acoustics of Propellers, AGARD CP-366, AGARD, Neuilly-Sur-Seine, France, 1985, pp. 12-1–12-24; also NASA TM-83733, Oct. 1984.

[2]Mehmed, O., Niskode, P., and Chen, T. W., "Flutter Results of CR Propfan Models," Advanced Turbo-Prop Workshop, NASA Lewis Research Center, Figure Set No. 4, Cleveland, OH, Nov. 1986.

[3]Mehmed, O., Kaza, K. R. V., Lubomski, J. F., and Kielb, R. E., "Bending-Torsion Flutter of a Highly Swept Advanced Turboprop," NASA TM-82975, Oct. 1982.

[4]Mehmed, O., and Kaza, K. R. V., "Experimental Classical Flutter Results of a Composite Advanced Turboprop Model," NASA TM-88792, July 1986.

[5]Crawley, E. F., and Ducharme, E. H., "Parametric Trends in the Flutter of Advanced Turboprops," American Society of Mechanical Engineers Paper 89-GT-280, June 1989.

[6]Turnberg, J. E., "Classical Flutter Stability of Swept Propellers," AIAA Paper 83-0847, May 1983.

[7]Kaza, K. R. V., Mehmed, O., Narayanan, G. V., and Murthy, D. V., "Analytical Flutter Investigation of a Composite Propfan Model," NASA TM-88944, April 1987; also *Journal of Aircraft*, Vol. 26, No. 8, 1989, pp. 772–780.

[8]Mahajan, A. J., Lucero, J. M., Mehmed, O., and Stefko, G. L., "Aeroelastic Stability Analyses of Two Counter Rotating Propfan Designs for a Cruise Missile Model," NASA TM-105268, April 1992.

[9]Balan, C., Sullivan, T., Fost, R., Hoff, G., Janarden, B., and Whitfield, C., "Modern Counter-Rotating Blade Concepts Performance Testing in NASA Wind Tunnels," Rept. GE TM87-528, NASA Contract NAS3-24080 Task V, Jan. 1990.

[10]Kurkov, A. P., and Mehmed, O., "Optical Measurement of Unducted Fan Flutter," American Society of Mechanical Engineers 91-GT-19, 1991 and NASA TM-103285, June 1991.

[11]Swallow, R. J., and Aiello, R. A., "NASA Lewis 8- by 6-Foot Supersonic Wind Tunnel," NASA TM-71542, May 1974.

[12]Delaney, B. R., Balan, C., West, H., Humenik, F. M., and Craig, G., "A Model Propulsion Simulator for Evaluating Counter Rotating Blade Characteristics," Society of Automotive Engineers 861715, Oct. 1986.

[13]Kurkov, A. P., "Optical Measurement of Propeller Blade Deflections," NASA TP-2841, Sept.1988.